Remote Sensing of Environment 113 (2009) 1067–1081

Contents lists available at ScienceDirect

Remote Sensing of Environment

journal homepage: www.elsevier.com/locate/rse

The structural and radiative consistency of three-dimensional tree reconstructions from terrestrial lidar

Jean-François Côté [a,*], Jean-Luc Widlowski [b], Richard A. Fournier [a], Michel M. Verstraete [b]

[a] Centre d'applications et de recherche en télédétection (CARTEL), Département de géomatique appliquée, Université de Sherbrooke, Sherbrooke, Québec, Canada J1K 2R1
[b] Global Environment Monitoring Unit, Institute for Environment and Sustainability, European Commission – DG Joint Research Centre, I-21020 Ispra (VA), Italy

ARTICLE INFO

Article history:
Received 16 October 2008
Received in revised form 25 January 2009
Accepted 31 January 2009

Keywords:
Architectural tree model
Terrestrial LiDAR
3D tree structure
Canopy reflectance model
Radiation transfer simulations

ABSTRACT

A novel methodology is proposed to reconstruct 3D tree architectures from terrestrial LiDAR (TLiDAR) scans. The methodology is robust and relatively insensitive to wind- and occlusion-induced artefacts in the 3D TLiDAR point clouds. A quantitative evaluation of structural attributes, like the vertical foliage and wood area profiles, as well as the shoot orientation distribution, was performed. Due to the difficulties of acquiring reliable and accurate estimates of these parameters in the field, an original evaluation approach was chosen that reproduces the TLiDAR scanning and subsequent tree reconstruction process in a virtual environment. In a second step the reconstructed tree models were ingested in a validated 3D radiative transfer model to simulate both their reflectance signatures (observable by space borne instruments) and directional transmission properties (measurable during field campaigns) under various spectral, illumination and tree density scenarios. The results of these evaluations confirm the appropriateness of the proposed tree reconstruction model for the generation of structurally and radiatively faithful copies of existing plant and canopy architectures.

1. Introduction

Due to their ability to capture the three-dimensional (3D) spatial arrangement and structure of vegetation canopies, terrestrial light detection and ranging (TLiDAR) systems have received a lot of attention in forest management, ecology as well as remote sensing and urban planning applications (Lovell et al., 2003; Chasmer et al., 2006; Omasa et al., 2007). TLiDAR systems record the 3-D position of objects within the scanner field of view by measuring the time delay between the transmission of a laser pulse and the detection of the return pulse reflected from the target. They can provide permanent 3-D records of canopy structure and detailed information about forest canopy architecture. TLiDAR have been used for estimating dendrometric parameters in forests (Simonse et al., 2003; Hopkinson et al., 2004), the leaf surface density of individual trees (Hosoi & Omasa, 2006) and to measure directional gap fraction of forest canopy (Danson et al., 2007) to name a few. Efforts have also been made to reconstruct the stem and branch structures from TLiDAR scans (e.g., Pfeifer et al., 2004; Cheng et al., 2007). Recently, Xu et al. (2007) developed an approach for producing polygonal models of trees reconstructed from TLiDAR scans. These efforts are nonetheless highly dependent of the quality (e.g. sampling frequency, scanning speed, etc.) of the scans acquired with TLiDARs. The reconstruction of wood and foliage elements can become difficult when the scans are of insufficient quality and this constraint has prevented an explicit regeneration of 3-D tree architecture so far. This is primarily due to the technical constraints of the scanning systems and the difficulty of overcoming adverse environmental conditions that exist during data acquisition. For example, TLiDAR scans made in natural forest environments usually require dealing with different levels of obstruction between the various vegetation components (Hopkinson et al., 2004). In addition, the presence of mild to moderate wind conditions will result in noisy results from TLiDAR scans due to the erratic motion of the smaller tree constituents (branches, twigs, foliage). The co-registration of multiple TLiDAR scans of a given tree object, acquired from different view angles, will thus lead to artificially dense 3D point clouds. Data post-processing techniques are required to deal with these and other issues that influence the quality of the end-product such as (i) the presence of structural elements that are finer than the resolving power of the laser scanner, e.g., individual needles in a conifer shoot, (ii) the lack of explicit information about leaf or shoot/needle inclination, and (iii) the spatial density of the laser beam per unit volume (Hosoi & Omasa, 2007).

Overcoming these difficulties would permit to have access to explicit descriptions of the 3D structure of plants, trees and entire canopies. This would also enable us to improve our knowledge in a whole range of applications ranging from fire risk modelling to forest management strategies, from light availability studies to carbon fixation processes, and from biodiversity indicators to water runoff modelling, to name but a few. Unfortunately, such detailed datasets that describe the 3D structure of entire canopies in an exhaustive

* Corresponding author.
E-mail address: Jean-Francois.Cote@USherbrooke.ca (J.-F. Côté).

0034-4257/$ – see front matter © 2009 Elsevier Inc. All rights reserved.
doi:10.1016/j.rse.2009.01.017

manner do not exist and these issues can only be addressed with statistical representations of plant and tree architectures (e.g. AMAP: Godin et al., 1999; L-Systems: Prusinkiewicz & Lindenmayer, 1990). Difficulties with representing tree architecture arise, however, when dealing with mature trees in complex environments where irregularities in recursive branching as well as the shedding of branches and their reorientation occur due to variable external factors that are difficult to quantify and/or predict (Runions et al., 2007).

In the context of optical remote sensing of forested areas, having access to detailed 3D tree and canopy architecture information of existing forest stands would enable a completely new approach to the validation of space borne measurements and derived products. For example, point clouds of forest canopies taken by a TLiDAR could be used in conjunction with validated radiative transfer (RT) models to evaluate current methodologies that convert local light transmission measurements into leaf area index (LAI) or the Fraction of Absorbed Photosynthetically Active Radiation (FAPAR) information. Alternatively, optimised sampling schemes could be devised, for individual long-term validation sites of remotely sensed data and products, which account for the structural specificity of that test site, its ambient lighting conditions as well as the choice of instrument used to perform the *in situ* measurements. In an attempt to move towards such RT model aided validation schemes, we propose to describe and evaluate a methodology that allows for the reconstruction of plausible 3D tree architectures (containing both wood and foliage elements) from a series of TLiDAR scans minimising the impact of adverse effects like wind and occlusion. The goal here is thus not to build identical copies of individual trees but rather to generate 3D tree architectures that are as close as possible to the observed individual trees, both in terms of their structural attributes as well as in terms of their reflected and transmitted light signatures.

The quantitative validation of the structural and radiative characteristics of reconstructed tree models is not a trivial task. To do this properly would require the gathering of vast amounts of geometric and spectral field data, as well as concurrently acquired and atmospherically corrected remote sensing measurements. Nevertheless, some of the structural parameters of interest would be very difficult (e.g., vertical leaf and wood area profiles) if not impossible (e.g., foliage orientation distribution) to measure accurately. Furthermore, measurement uncertainties associated with the reference dataset might prevent a conclusive comparison of the original and reconstructed structural/spectral properties. This would likewise prevent the effective comparison of simulated and measured canopy reflectance properties. Although activities to evaluate tree reconstruction model against (destructive) field measurements are underway, it was decided – for the purpose of this study – to evaluate both the structural and radiative fidelity of a series of reconstructed tree models without having to deal with unknown or ill-quantified sources of uncertainty in the reference dataset.

TLiDAR scans are made from several positions (from 3 to 5) to reduce the occlusion problem. Post-processing is applied to integrate the point clouds from all position into a consolidated point cloud. A tree model, hereafter called the 'reference', was reconstructed based on the consolidated cloud points of TLiDAR scans taken from in-situ trees. For the purpose of validation we propose a novel approach to produce a '*second generation*' tree model, the 'reconstructed' tree model. It is produced by using a ray tracing algorithm which simulates the measurement configuration of the original TLiDAR scans but on the reference tree model. Finally, the same tree reconstruction algorithm was applied to the reference trees to produce a new virtual reconstructed tree model. In this way the various structural properties of the reconstructed tree model generated from the simulated LiDAR point cloud may be compared in an unambiguous manner with the reference tree. Also, it is possible to obtain an unbiased evaluation of the proposed tree reconstruction technique, even for structural attributes that would be very difficult to measure in the field. This evaluation procedure can, however, still be taken one step further, namely, by ingesting the reference and the reconstructed tree models into a validated radiative transfer (RT) model that simulates their reflectance and transmission properties. Since these simulations will be performed under identical illumination conditions and with identical spectral and directional scattering properties of foliage, wood and background, any resulting differences can be directly attributed to the structural differences between the reference and the reconstructed tree models.

2. The tree reconstruction model

This section describes a modelling approach that enables the faithful reconstruction of three-dimensional tree architectures based on the use of point clouds from TLiDAR scans. More specifically, a series of 3D point clouds from TLiDAR scans were aligned and converted into a series of segments geometrically and topologically connected for the representation of a tree, taking both the wood and foliage components into account. To achieve this goal, the proposed algorithm uses the range (distance) and intensity information of the TLiDAR scans (i) to extract vital clues on the main branching structure of the tree (i.e., the shape of the trunk and the main branches), (ii) to use that skeleton to add other branches at locations where the presence of foliage is very likely, and (iii) to iteratively use the availability of light as a criterion to add foliage in the center of the crown where TLiDAR information is sparse or absent due to occlusion effects. As such, the proposed algorithm will not yield an *exact* copy of the original plant structure, but rather aims at minimising the impact of adverse factors – like wind, occlusions and the presence of sub-resolution structure elements – while delivering a faithful reconstruction of tree architecture from those scans. For example, even a weak breeze will move the finer branches and foliage elements of a crown. This, in turn, tend to result in a co-registered 3D point cloud that appears denser than the real tree crown (swaying branches and foliage elements at different *x,y,z* positions appear in several line scans of the TLiDAR dataset). Similarly, the natural tendency of foliage elements to grow outward and orient themselves towards the light source and their opacity in the spectral range of the TLiDAR inevitably prevents the light pulses from penetrating deeply in this portion of the canopy crown where leaf or needle density is appreciable. This can be remedied somewhat by acquiring multiple TLiDAR scans from different view angles. In conifers the individual foliage elements (needles) are often tightly grouped together into shoots which may not be resolvable with some of the current generation of TLiDAR, in particular if the trees are tall. Scanning tall trees generally requires locating the TLiDAR further away from the tree which results in reducing the effective resolution of the instrument and increasing the occurrence of obstructing objects. The tree reconstruction model that is proposed here is capable of overcoming or minimising many adverse factors. Fig. 1 illustrate the modelling process by showing a targeted tree, its co-registered 3D point cloud generated from three point clouds taken at different view points by a TLiDAR, and the reconstructed tree model.

Initial tests of the tree reconstruction procedure were done with TLiDAR scans from two coniferous forest sites, located in Canada and France, respectively. Four individual trees, belonging to 4 different coniferous species, were chosen to generate tree models that would subsequently serve as 'references' in the evaluation procedure of the tree reconstruction model (Section 3). The four coniferous trees were scanned with the TLiDAR Ilris-3D of Optech Inc. (www.optech.ca). This system operates at 1500 nm and scans within a maximum field of view window of 40 °×40 °. The beam divergence is 0.00974 ° and the minimal spacing between two beams is 0.00115°. The acquisition mode allows the recording of the first or last return 3D position as well as the intensity of the returned signal. A Douglas fir (*Pseudotsuga menziesii*), a western red cedar (*Thuja plicata*) and a western hemlock (*Tsuga heterophylla*) were scanned from Malahat and Shawnigan experimental sites (Vancouver Island, Canada) in October 2005. An Aleppo pine (*Pinus halepensis*) was scanned from the site of Bois-des-

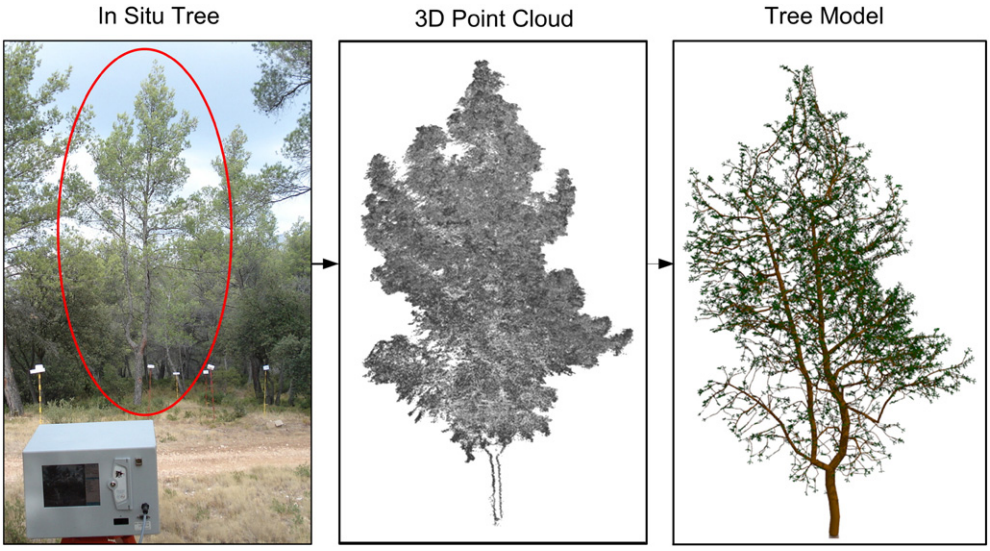

Fig. 1. [*Left*] Original photography and scanning configuration of an Aleppo pine tree with a terrestrial LiDAR Ilris-3D of Optech. [*Center*] Aligned Scans from 3 points of view. [*Right*] Computer generated tree model.

Roussettes (Aix-en-Provence, France) in September 2007. The number of scans per individual trees varied from 3 points of view for the western red cedar, western hemlock and Aleppo pine to 5 for the Douglas fir. If we normalize values at 15 m, all trees at the Malahat site (Douglas fir, western cedar and western hemlock trees) were scanned with a mean beam density of 3 mm, and the Aleppo pine were scanned at 4.7 mm. Depending on tree height, the TLiDAR scans were acquired at distances from 20 to 50 m from the target. First return acquisition mode was selected for all sites. The 3D point clouds taken by the TLiDAR from different view points were aligned into one geometric coordinate system with the software Pointstream 3DImageSuite (http://www.arius3d.com/). The alignment procedure for multiple points of views is done iteratively taking one reference viewpoint and adding gradually one other viewpoint at a time. An initial step matches at least 3 reference points common to both point clouds. Then in a second step, an alignment procedure, merges both individual point clouds into one aligned and registered (co-registered) point cloud using an iterative closest point algorithm developed by Besl and McKay (1992). From this new co-registered point cloud the same procedure is repeated iteratively for the remaining individual point clouds. The alignment accuracy provided by the software gave a root mean square error of less than 4 mm for all the co-registered point clouds.

The rest of the section explains the conversion of a 3D point cloud into coherent 3D tree architecture as illustrated in Fig. 2.

2.1. Branch structure generation

Once the multiple scans of a scene taken by a TLiDAR are registered and aligned, points were selected based on their intensity. Foliage tends to be darker than wood components because (i) foliage and woody material possess different spectral responses at 1500 nm where the reflectance signature of foliage is typically lower than woody bark material and (ii) most woody surfaces in such environments possess a larger contact area per laser pulse compared with leaves or conifer needles which thus do not reflect all incident pulse energy. Therefore selecting the brightest/darkest points of the 3D point cloud acquired select the returns associated to woody/foliage structures. The 3D point cloud N is thus divided into two subsets N_w and N_f for the wood and foliage components, respectively, where $N \supseteq N_w \cup N_f$. The selection of points was performed by using two different threshold values t_f, t_w, that were applied throughout the intensity image to select points belonging to wood (intensity $\geq t_w$) and foliage (intensity $\leq t_f$). The values of t_f, t_w were chosen manually according to the bright/dark criterion (mentioned above) only. Under natural conditions, it is difficult to infer typical reflectance values for foliage or wood material due to (i) specie-specific spectral response and (ii) variability in surfaces' orientation which changes the preferred direction of the reflected pulse energy. The choice of two different threshold values resulted in the removal of points with intensity between t_f and t_w ($t_f < t_w$). If necessary, further processing of the point cloud N_w may remove outliers, noise and unwanted parts by using manual selection tools available in Pointstream 3DImagesuite. It might also be required to fill in or repair some important parts to the main branching structures (e.g., trunk, main bifurcations, etc.) that have been under-sampled due to external conditions (e.g., winds, object occlusion). This procedure consisted in adding points on the under-sampled object surface using tools available in Pointstream 3DImageSuite such as to have the 3D surface of the scanned object sampled in an exhaustive manner. Obviously the same process can also be applied to N_f.

The point cloud N_w then served as input to the skeletal curve extraction algorithm adapted to handle the noisy point cloud through to the use of adjustable parameters. Further details on this algorithm can be found in Verroust and Lazarus (2000). In brief, the algorithm generates connected curves that are organized like a tree from the scattered 3D point cloud N_w. A neighbourhood graph is built on N_w, where every point in N_w is attached to k nearest neighbors. The value of k is set to produce realistic skeleton silhouettes of trunk-branches patterns. In a further step, the Dijkstra algorithm (Cormen et al., 2001) is used to find the shortest path between a pre-selected root point (in N_w) acting as the source point and every other point in N_w. The algorithm returns the paths and the Euclidean distance separating the root point and one another point which are called geodesic distance. A series of level sets composed of all the points located at the same geodesic distance are extracted to be structured as a tree data structure. To do so, skeletal curves are built across the centers of each level sets (called node sets) to generate a primary skeleton composed of the trunk and some principal branches. This skeleton is an oriented (i.e., from the root to the tree top) tree structure (V, E), with V being the x,y,z center locations of the connected node sets and E being the vectors (called edge sets) linking two subsequent node set centers.

Building the branching structure depends on a set of attractors $A \subset N_f$ chosen as input to an algorithm of colonization that is described in Runions et al. (2007). An attractor represents an empty region where one or multiple branches can grow. The ensemble of TLiDAR

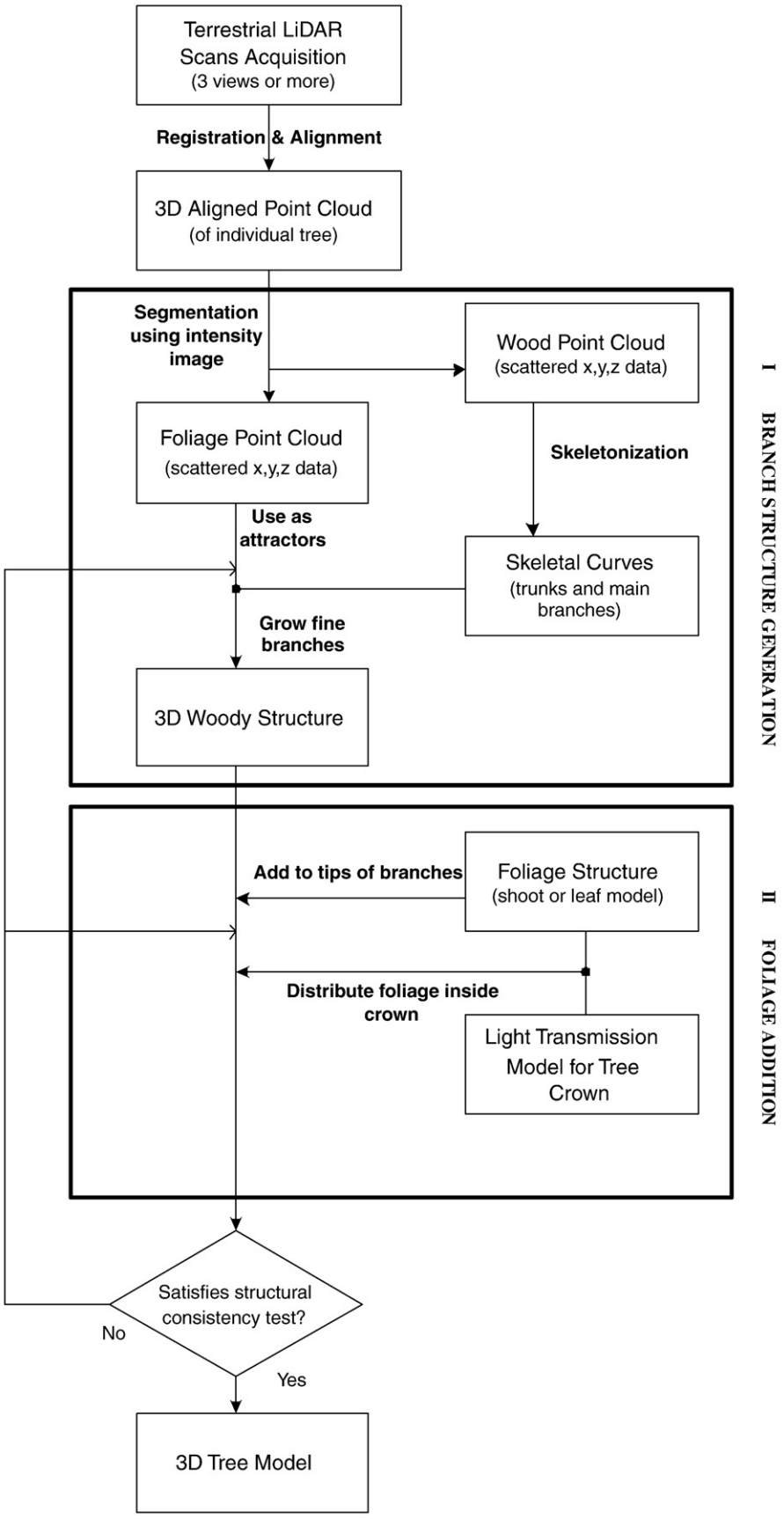

Fig. 2. Conceptual diagram of the modelling approach.

points identified as N_f are ideally suited to act as attractors since branches can be expected to grow towards volumes where foliage is identified. The logic behind this is to assume that branches support foliage thus the amount of final branching structure of a reconstructed tree is proportional or is 'attracted' by the amount of foliage points. Parameters of the algorithms allow modifying the spatial distribution of branches within the empty space. The number of attractors has an effect on the density of branches with fewer attractors leading to a sparser branching structure. The algorithm operates over all attractors $a \in A$. At each iteration, an attractor a influences a node $v \in V$ if the distance between a and v is less than a radius of influence d_i. This radius controls the distance from which a branch can sense the influence of an attractor. Generally speaking, an absolute decrease of the radius d_i results in a wavy skeleton while relatively high values of d_i results in a skeleton with long straight segments. The set of attractors influencing a node v is denoted as $S(v) \subseteq A$. If $S(v)$ is not empty, a new node $v' = v + D\hat{n}$ is attached to v with a segment $e = (v, v')$, where

$$\hat{n} = \frac{\vec{n}}{||\vec{n}||} \text{ and } \vec{n} = \sum_{s \in S(v)} \frac{s - v}{||s - v||} \quad (1)$$

When all new nodes are attached to the branching structure, the algorithm removes the attractors whose distance from the closest node (segment) is lower than a threshold distance d_k. This threshold controls how close a branch can get to an attractor. Thus decreasing d_k favours the addition of small branches and twigs while increasing d_k leads to a smoother and sparser skeleton. Each new node v' and segment e contribute to augment the skeleton (V, E), with $V = V \cup v'$ and $E = E \cup e$. This procedure is repeated until the set of foliage attractors A is empty; it generates the main branching structure that will subsequently support the foliage, as well as a few additional minor branches if necessary. The radius r of each branch is calculated following the pipe model, where the cross-sectional area of a branch equals the sum of cross-sectional area of its c child branches:

$$r^P = \sum_{i=1}^{c} r_i^P \quad (2)$$

where r_i is the radius of the ith children and P ranges generally between 2.49 and 3 for mature trees (Shinozaki et al., 1964; Taylor-Hell, 2005).

Exploiting intensity and range information from TLiDAR point clouds in conjunction with algorithms to generate tree skeletons thus yields a plausible reconstruction of a tree's branching structure.

2.2. Addition of foliage to the branch structure

The next algorithm step for the tree reconstruction model deals with the addition of foliage around the newly generated skeleton various branch segments. Foliage properties differ from species to species and depend also on the age of the plant (young vs. mature) as well as on external environmental factors (e.g. water content and nutrients). The four tree species that were used in this study are all conifers. However, rather than using four different needle and/or shoot structures, a generic conifer shoot structure (Fig. 3, inlaid panel) was used for all 4 species. This was partly justified by the lack of detailed information concerning actual shoot structures and by the virtual context in which the tree models were evaluated. The shoot structure used in this study was composed of four elements: 1 "mature" shoot supporting 3 new shoots attached with branching angle chosen as −50°, 0° and 60°. The structure for each of the four elements follows the model of Smolander and Stenberg (2003) and features identical numbers of needles (190). The mature shoot had longer (15 vs. 7.7 cm) and broader (3 vs. 1.5 mm radius) needles than the three young shoots. The needle spatial distribution of one shoot assumed [i] a constant radius (0.46 mm) and length (2.85 cm) of the shoot's central twig, [ii] a constant angle between the shoot's axis and a needle (40.5°), and [iii] a constant fascicle angle between pairs of needles (40.5°). The angle distribution around the axis followed a Fibonacci sequence with a divergence angle of 8/13*2π. That shoot structure was reused for all conifer trees to reduce the requirements already high for computer memory.

Before adding the foliage, the branching structure created in Section 2.1 was translated into a format compatible with an open L-System growth grammar (Měch & Prusinkiewicz, 1996). L-Systems served to encode and represent the architecture of the plant. The L-System growth grammar consists of two sets of production rules that are applied to all branch segments in order to add the foliage. The first set of production rules assumes that every tip of a branching structure supports foliage, since the attractor points used to grow the branch structure corresponded in all likelihood to actual foliage elements. The second set of production rules adds new shoot structures according to the light availability at the center point of a given segment in the crown. The latter is evaluated with a simple light transmission model computing the number of gaps that exist above a given segment's position. To do this, the scene is partitioned with a tight 3D matrix of small voxels (here, $0.3 \times 0.3 \times 0.3$ m^3), where each voxel can be characterized by the plant properties (such as area density) within its volume. Light sources are positioned on a horizontal plane above the tree crown. A ray is launched from the center point of the segment to the direction of each light source position, and the probability of obstruction P_O is computed in accordance with a Beer's law, assuming a spherical angular distribution of canopy elements:

$$P_O = 1 - \prod_{\text{voxel}} exp[-S_{\text{voxel}} \cdot D_{\text{voxel}} / 2] \quad (3)$$

For each voxel hit by a ray at zenith angle θ, D_{voxel} is the plant area density and $S_{voxel} = z/cos(\theta)$ is the path length of the ray, with z being the projection of the path onto the vertical direction. We assign a gap if $P_O < U$, with U being a random variable in the interval [0, 1]. The number of light sources or maximum number of gaps viewable from the segment's location was set to 9 as a compromise between the simulation accuracy of the light transmission model and computation time. We obtained visually realistic results by adding new foliage elements when 6 out of the 9 available light sources were visible without obstruction (i.e. through gaps) from the segment. In that case, our criterion was based on the visual aspect of the foliage repartition within the tree crown according to the original photography of the tree. All new shoots were randomly rotated before being attached to the location of the segment. Despite the simplified nature of this light transmission model, it enabled practical addition of foliage in the center of a tree's crown on a defendable principle, where information on the distribution of objects is often not available from the 3D point cloud taken with the TLiDAR. Unfortunately, both the occurrence of wind and occlusions prevented the use of the subset point cloud N_f as a criterion 1) to end the process of foliage addition inside the tree crown, and 2) to evaluate the faithfulness of the foliage distribution within the tree crown (and also for the entire tree reconstruction process). Therefore the proposed tree reconstruction model used either a qualitative (e.g., visual match appearance) or quantitative (e.g., leaf area match) constraint to terminate the foliage addition process.

The four trees that were scanned with the TLiDAR Ilris-3D were rebuilt with the methodology described in Fig. 2. Fig. 1 shows firstly the reference Aleppo pine tree target in the forest with secondly the co-registered 3D point cloud generated from the first returns of three TLiDAR scans of the reference Aleppo pine, and thirdly the reconstructed Aleppo pine tree architecture. Differences between the reference tree and the aligned 3D point cloud are clearly apparent and result from the moderate wind conditions during the three TLiDAR acquisitions. Nevertheless, the proposed reconstruction

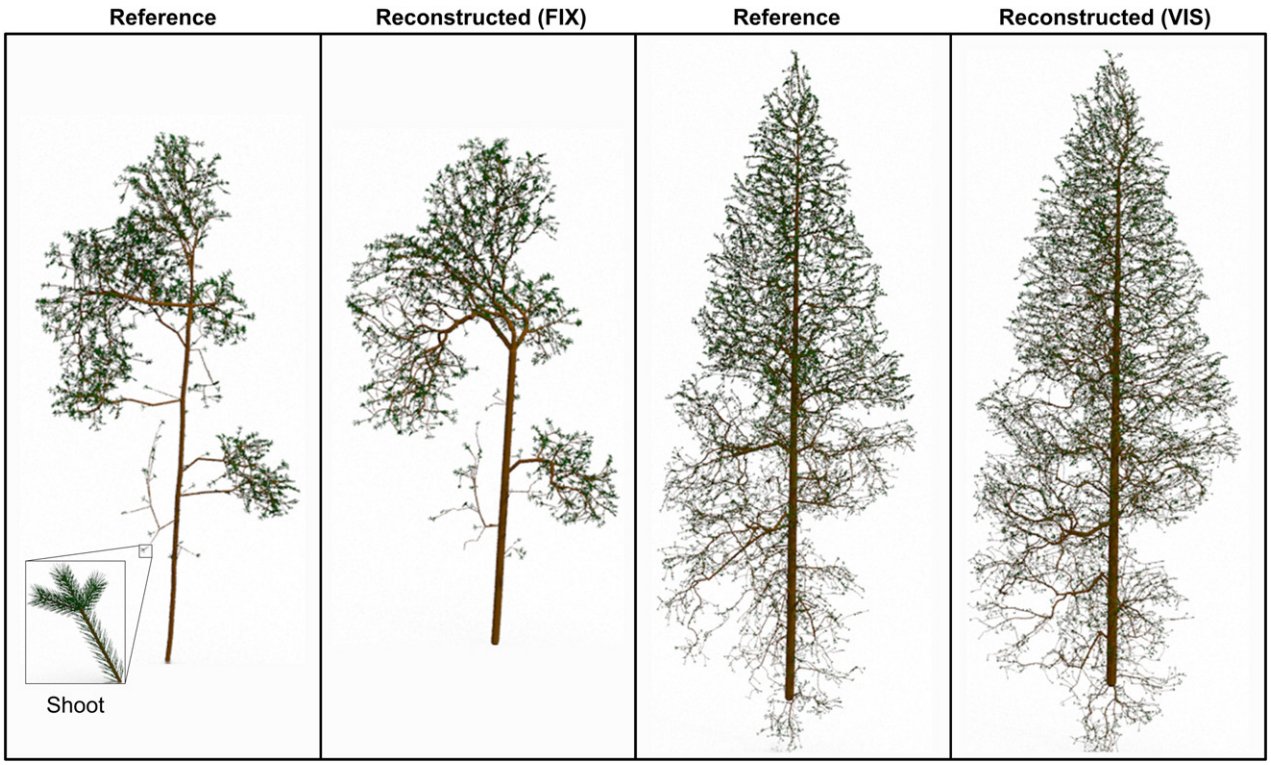

Fig. 3. Examples of tree models. *[Left]* Reference western hemlock tree model and reconstructed tree model using a fixed number of shoots to terminate the foliage addition process (FIX). *[Right]* Reference western red cedar tree model and reconstructed tree model using a visual comparison (VIS) to terminate the foliage addition process. [*Inlaid*] Shoot structure that was used in all tree models.

algorithm was able to produce a visually faithful reconstruction of the overall Aleppo pine tree structure, despite these unfavourable measurement conditions.

3. Evaluation of architectural tree properties

Rigorous evaluation of the tree reconstruction procedure would require access to an exhaustive list of structural attribute values of the reference tree. The structural characteristics are of particular interest here because of their significant role in the context of canopy reflectance modelling of forested targets, i.e., woody content, foliage area, foliage orientation and distribution. Unfortunately, no dataset exists with the exact *x,y,z* location (and orientation) of individual foliage elements, twigs, and branches in a tree. We overcame this limitation by simulating the 3D point cloud of the TLiDAR scans for the reconstructed trees. This way to proceed generated a set of 'second generation' trees for which we could compare all structural details with the original version of the reconstructed tree model.

To do so, a series of 3D point clouds from TLiDAR scans were simulated on the four reference tree models in an attempt to evaluate how the proposed tree reconstruction model matched the proportions, distributions and orientations of wood and foliage constituents. Using the PBRT (Physically-Based Ray Tracing) ray tracing software (Pharr & Humphreys, 2004) allowed to simulate the perspective of a camera with a field of view of $40° \times 40°$ identical to the one that is used by the Ilris-3D TLiDAR system. Rays were launched from the simulated camera for each pixel of the image. In practice, each laser beam of the Ilris-3D was simulated by launching 9 individual rays uniformly distributed within the pulse's divergence angle. The disadvantage of this technique is that the density of rays reaching an object decreases with the distance from the laser source position and increases the distortion/artifacts known as aliasing when representing a high-resolution signal at a lower resolution. However, this approach considerably simplifies the simulations compared to cone ray tracing technique (Amanatides, 1984). First hit position of the rays on the tree model were recorded and subsequently treated as the first return from the TLiDAR return signals. The tree model was placed at a distance such that the camera could see the entire tree. The foliage material was configured to provide a return with lower intensity compared with the woody material. Three TLiDAR scans were simulated at azimuth angles of 0°, 120° and 240° around each tree, leaving the distance between the camera and the tree model constant. Each simulated scan produced a raster image 1050×1050 of the first returns equivalent to an angular/spatial resolution of 10 mm at a distance of 15 m. Each of the four tree were generated from 3 simulated point clouds that were registered and aligned in order to generate an integrated 3D point cloud that could serve as input to the tree reconstruction model.

The input parameters $\{d_i, P, A, d_k\}$ were chosen from a visual comparison of the generated pictures of the models with the photographs taken on the test sites (see examples in Fig. 3). In practice, the final branching structure was less sensitive to the parameter d_i, but was more responsive to the variation of the three other input parameters of the colonization algorithm: (i) the pipe model parameter P that controls the radius (dimension) of branches, (ii) the attractor set A and (iii) the radius d_k. The amount of foliage added on the model tree was determined in two ways: either the number of shoots was chosen such as to minimise the visual differences between the reconstructed and reference tree models (this approach will be labelled as VIS), or, the number of shoots was forced to match that of the reference tree models (this approach will be labelled as FIX). In essence, the former case assumes that ancillary information about the tree is unavailable while the latter assumes that the number of foliage elements in the tree crown could be approximately estimated from allometric equations (depending on their availability and accuracy). A visual comparison takes place (i) for branching structure of VIS and FIX reconstructed tree models and (ii) during foliage addition for the VIS reconstructed model. The visual similitude between models is evaluated on the following criteria: 1) overall crown density when superposed over a white or identical

background (see Fig. 3) and 2) the spatial distribution of branches as well as their dimension (radius) and the amount as well as the spatial distribution of foliage. The reconstruction ends when these two criteria are visually matched between the reference and the reconstructed tree models from visual criteria.

At the end of this reconstruction process, both the reference and reconstructed tree models are exported into the scene description formats required by the PBRT renderer (Pharr & Humphreys, 2004) and the Rayspread radiative transfer model (Widlowski et al., 2006). In doing so, each branch segment is represented as a truncated cone to facilitate the computation of surface areas, orientations and volumes that are required in a forest canopy models for remote sensing. Fig. 3 shows two image pairs of reference and reconstructed tree models for western hemlock (left) and western red cedar (right) trees. The proposed methodological setup thus allows (i) a detailed comparisons of the structural attributes of the reference (representing the truth) and the reconstructed tree models, and (ii) an estimation of the impact that such differences might have on the reflectance properties of entire forest canopies.

3.1. Evaluation of the scanned 3D point clouds

The first evaluation of the reconstructed tree model involved the comparison of the VIS and FIX reconstructed tree models using the same three scanning positions. The spatial/angular resolution of the simulated model matched those from the scans made with the TLiDAR to generate the reference tree model. The aligned 3D point clouds of the reference and the FIX/VIS reconstructed tree models were encompassed into a 3D matrix of voxels having 0.3 m side length. This allowed to compare properties of each tree model types (such as the number of LiDAR returns in each voxel). Fig. 4 shows the distribution of the normalised difference in the return numbers per voxel that were observed between the reference tree model and either the VIS (black circle) or the FIX (grey diamond) reconstructed tree models. Also indicated are the mean normalised differences and their standard deviations for the four trees. The norm value is defined by $\max_i |difference_i|$. All distributions in Fig. 4 are mono-modal with peak values close to zero and a standard deviation less than 0.17, which indicates that a high amount of voxels have very similar numbers of returns in both the reference and the reconstructed tree models. Branches and leaves of the reconstructed tree models are therefore distributed similarly to those in the reference tree model. Overall, however, the mean values are all slightly higher than zero (0.008 to 0.011), except for the Douglas fir tree where it is slightly below zero (−0.004 to −0.002). This can be explained by the fact that all reconstructed tree models (except for the Douglas fir) have a higher wood area value than their respective references and also a higher leaf area value (except for the VIS reconstructed western red cedar tree model).

Table 1 compares volumes of the convex hull of the reference tree with the VIS and FIX reconstructed tree models. The convex hull volume was computed using the software Qhull (Barber et al., 1996) with every object position in the tree. The volume was not only computed with objects from the living crown but also with points from the bottom part of the trunk. It is therefore a quantity linked to the volumetric spatial extent of the whole tree which is rather sensitive to the presence or absence of individual branches. From the comparison we observed that the reconstructed tree models produce a convex hull volume relatively similar to those of the four reference tree models with deviation from 4.7 (for the Douglas fir tree) to 24.9% for the western hemlock tree. In all cases, the convex hull volume of the reconstructed tree model exceeded that of the reference tree model. This positive deviation indicates that the parameter configuration of the attractors set A and the radius d_k led to somewhat bigger trees – a fact that was not necessarily apparent during the visual evaluation of the reconstructed tree pictures. At the scale of an individual tree, the internal 3D architecture of the foliage and branching system has more impact on the reflectance signature than small differences in the length of individual branches, in particular when a given canopy is viewed with medium resolution optical passive remote sensing data used in global applications (e.g. MODIS, MERIS, and MISR). More specifically, a small set of key structural parameters, like the spatial distribution of the foliage and wood area as well as the orientation of the various foliage elements, are capable of substantially altering the directional reflectance signature of vegetation targets.

3.2. Comparison of structural attributes

Foliage area and orientation are both crucial state variables controlling the radiative properties of vegetated surfaces. Increasingly, the woody area is also sought after as an input parameter to canopy reflectance models as well as climate change models. From the comparison of the total leaf and wood area between the reference and reconstructed (VIS and FIX) tree models for the four trees (Table 2), we found deviations similar to those observed for the hull volume. Throughout this study such differences are expressed in percent and are computed as:

$$\Delta = \frac{100}{N}\sum_{i=1}^{N}\left(\hat{y}_i - y_i\right)/y_i \tag{4}$$

where N is the number of values to average over, $\hat{y}_i$ is the value of the reconstructed tree model parameter of interest, and y_i the reference value of the reference tree model. Here the parameters of interest are the total foliage area and total wood total area calculated by summing each object's total surface area of foliage and wood component respectively.

Deviations in leaf area range from −6.8 to 19% and were largest for the visually reconstructed Aleppo pine and Douglas fir tree models. Obviously, null deviations in foliage area were observed for the FIX reconstructed models since here the number of shoots in the reference and reconstructed tree models was imposed to be the same. Similar deviations in wood area values were observed but were generally larger for the VIS reconstructed tree models. This is explained by the fact that the addition of individual conifer shoots increased the woody area of a tree due to the central twig that was contained in a shoot. This effect can be seen even with tree crowns with relatively less foliage such as for the western hemlock and Aleppo pine trees.

The ability of the proposed architectural model to reproduce the vertical profile of leaf/wood area and leaf normal distribution was also assessed. The vertical profiles of leaf and wood area were generated by summing the area of the elements (wood or foliage) that fell within 1 m height bins. For simplicity, it was assumed that an object belonged to a height bin if its center of mass was contained within the height interval associated to that bin. Figs. 5 and 6 show the vertical profiles of leaf and wood areas, respectively, for the four different tree species that were used in this study. The vertical profiles of the reference tree model (solid line) are shown with those of the VIS and FIX reconstructed trees. The root mean squared deviation (RMSD) is reported as an indicator of agreement between the reference and the reconstructed trees. The RMSD was computed as:

$$\mathrm{RMSD} = \sqrt{\frac{1}{N-1}\sum_{i=1}^{N}\left(\hat{y}_i - y_i\right)^2} \tag{5}$$

where N is the number of values to average over (here N is the number of height bins), and $\hat{y}_i$, and y_i are the values of the parameter of interest for the reconstructed and reference tree models, respectively (here the parameter of interest is the amount of leaf area or wood area in a given height bin).

Overall, the vertical leaf and wood area profiles of the reconstructed tree models agree rather well with those of the reference tree

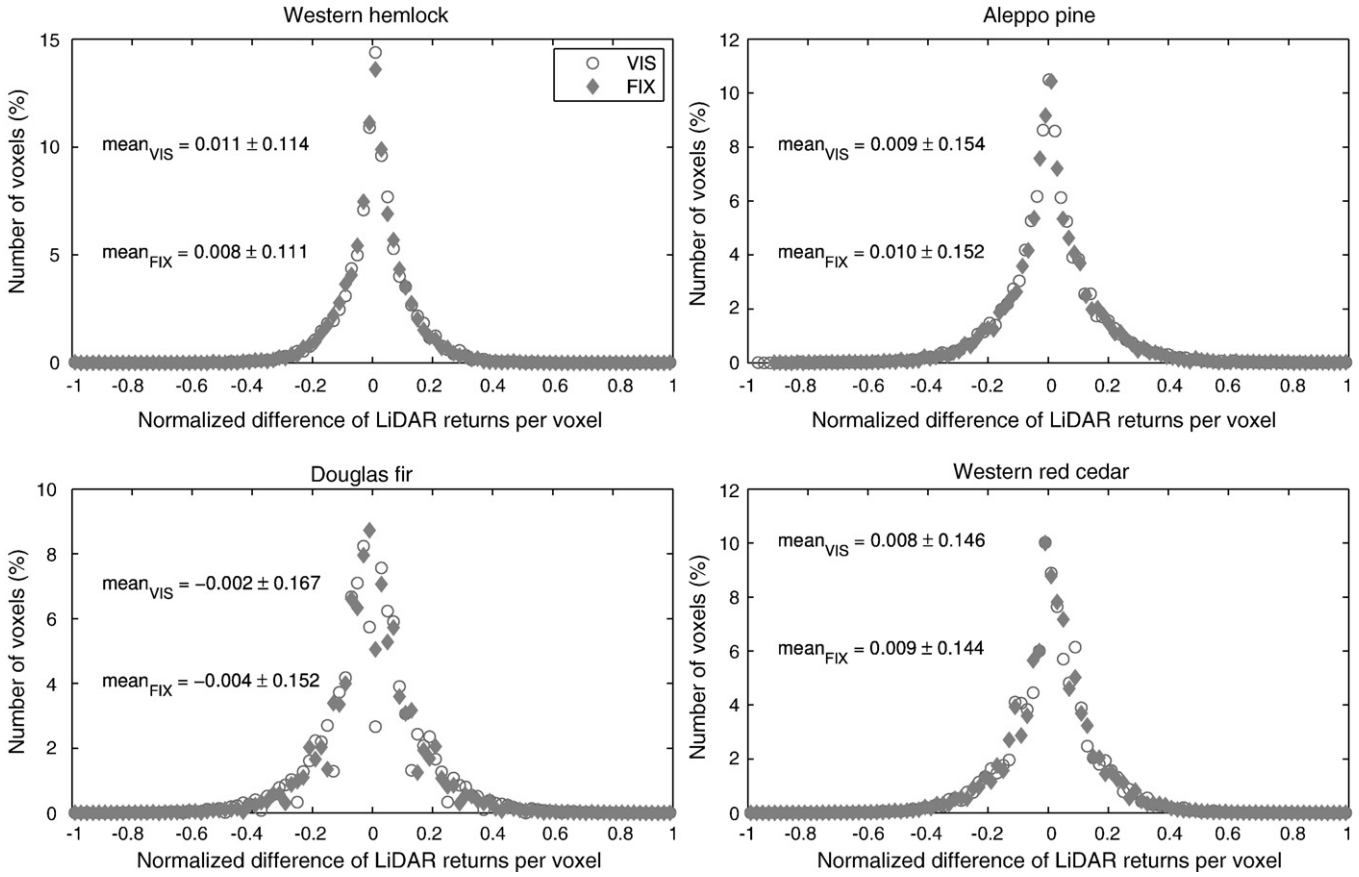

Fig. 4. Distribution of the normalized difference of LiDAR first returns per voxels for each reconstructed tree model: western hemlock (top left), Aleppo pine (top right), Douglas fir (bottom left), western red cedar (bottom right). The difference is calculated between the reconstructed and reference tree models and normalized with the highest absolute difference values. Mean value and standard deviation of the distribution for the visually compared (VIS) – white disk – and fixed number of shoots (FIX) – grey diamond – reconstructed tree models are displayed.

models. The graphs in Figs. 5 and 6 exhibit small differences in wood area profiles between the FIX and VIS reconstruction approaches, and show similar spatial distribution in foliage and wood area. For instance, both the FIX and VIS reconstructed tree models feature the same overall branching patterns and their woody area differs primarily due to the number of shoots that each contains an additional twig (wood material). In general, the reconstructed profiles 1) followed the overall leaf and wood area distributions of the reference, 2) matched the location of the maximum values and 3) showed only small differences at the top and bottom of the tree crowns. One exception to this behaviour is the Aleppo pine tree reconstruction, where the VIS model significantly overestimated the leaf area at the lower center of the crown (and both the VIS and FIX models had larger wood area values compared with the reference tree model). A closer inspection of the recreated tree models shows that the foliage surplus of two thick branches in the reconstructed tree crown was responsible for most of these discrepancies. This finding underlines a potential weakness for the use of visual consistency as it may depend on the particular viewing geometry at which tree models were compared. In the future, a more quantitative consistency check is certainly needed, not only to terminate the shoot addition process but also to evaluate the accuracy of the reconstructed tree architecture.

Foliage orientation is usually assumed to follow predefined statistical distributions rather than explicit measurements due the complexity of obtaining such datasets (Bunnik, 1978; Goel & Strebel, 1984; Campbell & Norman, 1990). Defining a methodology that retrieves foliage orientation would be of great interest, in particular for the canopy reflectance modelling community. Fig. 7 exhibits the distribution of the zenith angles of the shoot axes for all foliage elements contained in the crowns of the reference tree (black), FIX (grey) and VIS (white) reconstructed tree models. Each coloured bar corresponds to a 10° zenith angle interval ranging from 0 to 180°. The RMSD of the FIX and VIS zenith angle distributions were calculated with Eq. (5). The western red cedar tree yielded the best fit among the reconstructed tree models, having comparable RMSD values for both the VIS and FIX cases. The reconstructed Douglas fir models, on the other hand, showed a substantially larger amount of shoots with zenith angles in the range from 40° to 60° compared with the reference model. This can be attributed to the fact that the top part of the trunk of the Douglas fir was not visible in the TLiDAR point cloud due to occlusion. The local lack of measurements forced the branches that were added around the trunk at this location to grow upward in an attempt to reach out towards the attractors that were located in the

Table 1
Convex hull volume of the tree and deviation values for the reference and for the visually compared (VIS) and fixed number of shoots (FIX) reconstructed tree models.

	Convex hull volume (m^3)			Deviation of tree volume (%)	
	Ref	*VIS*	*FIX*	*VIS*	*FIX*
Western hemlock	130	163	162	24.9	24.5
Aleppo pine	183	215	215	17.3	17.2
Douglas fir	1145	1205	1200	5.2	4.7
Western red cedar	1610	1801	1806	11.9	12.2

Table 2
Leaf and wood area integrated over the entire tree and deviation values of the tree for the visually compared (VIS) and fixed number of shoots (FIX) reconstructed tree models.

	Leaf area (m^2)			Wood area (m^2)			Deviation of leaf area (%)		Deviation of wood area (%)	
	Ref	VIS	FIX	Ref	VIS	FIX	VIS	FIX	VIS	FIX
Western hemlock	112	123	112	44	54	52	9.6	0.0	24.8	19.9
Aleppo pine	207	246	207	87	104	96	19.0	0.0	19.0	10.1
Douglas fir	568	492	568	299	254	269	−13.3	0.0	−15.0	−10.0
Western red cedar	792	738	792	361	415	425	−6.8	0.0	14.9	17.8

upper parts of the tree crown. From this situation we found that the quality of the point cloud is the main factor influencing the distribution of shoot zenith angles since it leads the reconstruction algorithm's to extract the primary skeleton to support secondary branches.

The overall agreement of the vertical profiles of both leaf and wood area, as well as the shoot zenith angle distribution of the reconstructed and reference tree models, support the use of the proposed tree reconstruction procedure in retrieving structural vegetation attributes from TLiDAR scans. The quality of the point cloud as well as the nature of the architectural consistency tests (qualitative versus quantitative) had clearly an impact on the accuracy of the reconstruction of individual trees. The qualitative visual comparison criterion used to configure the parameters of the reconstruction model at the individual tree level should ideally be used in conjunction with an external source of information to best assess suitable model parameters (like the amount of foliage and its spatial distribution within the crown).

4. Evaluation of radiative canopy properties

For remote sensing observations, structural properties such as the foliage area and orientation influence the interactions of radiation incident on vegetation canopies and thus also the signal measured by remote sensing instruments. Assuming accurate knowledge of physical properties of the canopy constituents, state of the art RT models are capable of simulating both domain-averaged radiative properties (e.g., canopy albedo, bidirectional reflectance, or FAPAR), at spatial resolutions comparable to current medium spatial resolution sensors, as well as local point measurements (e.g., light transmission and background reflection) at any given location within a canopy. 3D radiative transfer models, if properly validated, are ideally suited for ground based validation of remotely sensed products. This is particularly relevant in comparisons with in-situ measurements since the latter almost always infer canopy properties from a series of spatially disjoint transmission measurements at the bottom of the forest canopy whilst remote sensing algorithms aim at retrieving the same canopy properties using reflected radiation quantities from a much broader canopy target. This section will document the differences between point- and domain-averaged reflectance properties, as well as between local directional transmission characteristics for forest canopies composed of the reference tree model versus the FIX and VIS reconstructed tree models.

4.1. Comparison of canopy reflectance signatures

The 3D Monte Carlo ray-tracing model *Rayspread* (Widlowski et al., 2006) was used to simulate bidirectional reflectance factors (BRF) i) over 250 uniformly distributed directions in the upper hemisphere

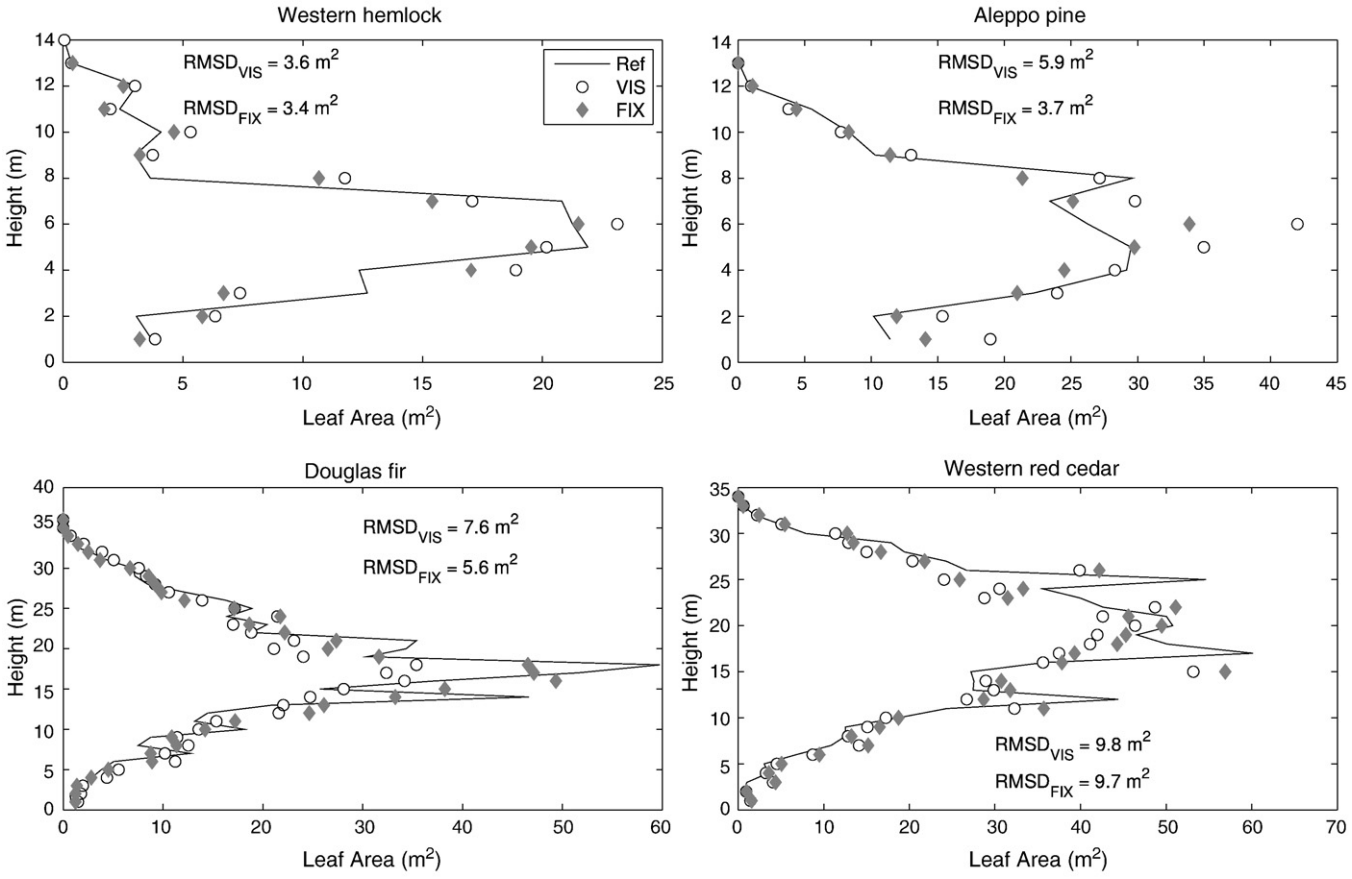

Fig. 5. Vertical profile of leaf area for 4 tree species: western hemlock (top left), Aleppo pine (top right), Douglas fir (bottom left), western red cedar (bottom right). Root mean squared deviations (RMSD) of the distribution are displayed for the visually compared (VIS) – white disk – and fixed number of shoots (FIX) – grey diamond – reconstructed tree models.

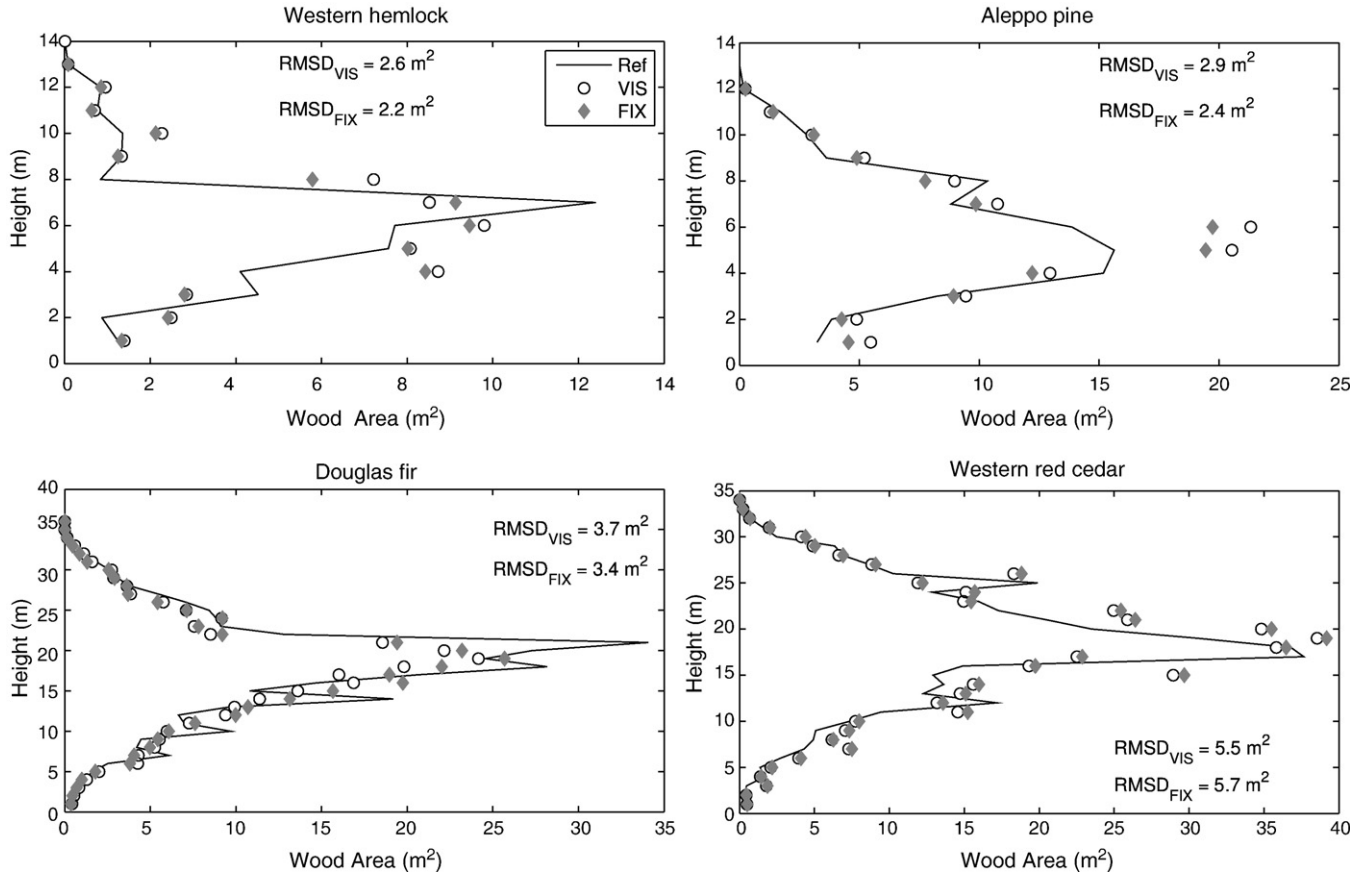

Fig. 6. Vertical profile of wood area for 4 tree species: western hemlock (top left), Aleppo pine (top right), Douglas fir (bottom left), western red cedar (bottom right). Root mean squared deviations (RMSD) of the distribution are displayed for the visually compared (VIS) – white disk – and fixed number of shoots (FIX) – grey diamond – reconstructed tree models.

and ii) at intervals of 5° zenith angle along the principal plane (containing both the local vertical and the illumination direction) for a variety of forest densities, spectral bands and illumination conditions. The Rayspread radiative transfer model has been extensively validated during the RAdiative transfer Model Intercomparison (RAMI) exercise (Pinty et al., 2001, 2004; Widlowski et al., 2007) and was recently chosen as one of the six 3D Monte Carlo models that contributed to the establishment of a "surrogate truth" reference dataset for the automated evaluation of new or updated canopy reflectance models (Widlowski et al., 2008).

The spectral properties for the soil, wood and foliage elements in the red and near-infrared (NIR) wavelengths were all taken from the RAMI third exercise (Widlowski et al., 2007). In the red spectral band, the values for leaf reflectance and transmittance were set to $r_l = 0.0546$ and $t_l = 0.0149$, respectively, while the reflectance of the wood was $r_w = 0.14$ and the background albedo was set to $\alpha = 0.127$. In the NIR, the corresponding values were $r_l = 0.4957$, $t_l = 0.4409$, $r_w = 0.24$ and $\alpha = 0.159$. A series of virtual 1 ha wide forest stands were built using two different scenarios: (i) one single tree was cloned and distributed randomly over the stand area and (ii) all four trees of our simulation set were cloned and distributed at random over the 100×100 m^2 area. In both cases, a random azimuthal rotation was applied around the vertical axis of each tree in order to avoid spurious frequencies in the scene. The position of this axis of rotation was determined by the center point of the rectangle enclosing the horizontally projected 3D TLiDAR point cloud of a given tree model. Slight differences in the spatial distributions of trees (and thus also in the simulated BRFs of a given forest canopy) were anticipated since the *x,y* coordinates of this center point changed between the reference and reconstructed tree models (especially for scenario (i) where the same tree species was systematically used to populate the scene).

With the forest creation scenario (i), three sites with fractional covers of approximately 20%, 40% and 60% were built for each one of the reference, VIS and FIX reconstructed tree models. For each one of these 9 structural cases, radiation transfer simulations were subsequently performed at three sun zenith angles (0°, 30° and 60°) and two wavelengths (red and NIR). Table 3 indicates the overall differences between the reconstructed and the reference BRFs (averaged over the 250 BRF simulations for all stand densities, spectral regimes and illumination conditions). The maximum recorded BRF difference was 7.44% in the red spectral band for the western hemlock tree. On average, however, the absolute BRF differences were 4.32% (2.15%) for the VIS and 3.74% (1.52%) for the FIX reconstructed tree models in the red (NIR) spectral band, when summed over all tree species. Multiple-scattering in the NIR results in lower BRF deviations than in the red spectral domain, which is dominated by single-scattering interactions and thus more sensitive to changes in the architectural properties of the trees.

In the second forest creation scenario, 100 instances of trees were chosen at random from among the four tree species and subsequently distributed throughout the 1 ha area. This process was done with the reference, VIS and FIX reconstructed tree models. Overall, a fractional cover of about 54% was obtained as estimated by summing the values of the projected elliptical surface (minor radius, major radius) of each tree crown and dividing this sum by the area of the forest stand. Overlaps between tree crowns were avoided by constraining each tree to be separated from its neighbours by a distance at least equal to their respective crown major radius (projected on the ground). The final forest canopies thus included 22, 16, 34 and 28 instances of the

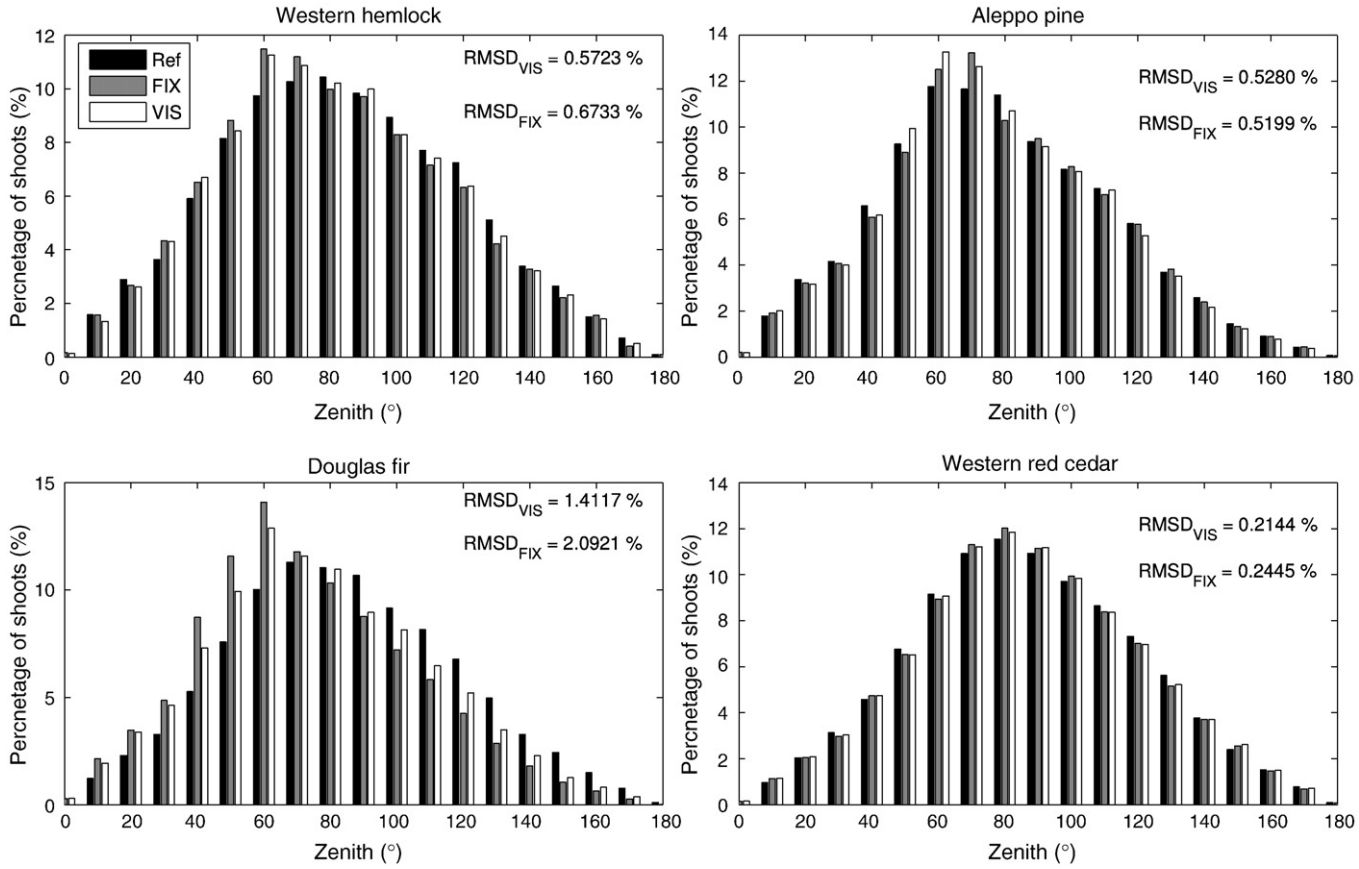

Fig. 7. Distribution of the zenith angle of the shoot axis (twig) area for 4 tree species: western hemlock (top left), Aleppo pine (top right), Douglas fir (bottom left), western red cedar (bottom right). Root mean squared deviations (RMSD) of the distribution are displayed for the visually compared (VIS) – white – and fixed number of shoots (FIX) – grey – reconstructed tree models.

western red cedar, Douglas fir, western hemlock and Aleppo pine tree models, respectively. Radiation transfer simulations in the red and NIR spectral regimes were carried out for each one of the three forest stands (reference, VIS and FIX), setting the solar zenith angle to 30 °. Fig. 8 shows the verisimilitude of the BRFs generated for a canopy composed of reference (solid line) as well as VIS (black circle) and FIX (grey diamond) reconstructed tree models, both in the red (left panels) and NIR (right panels) spectral regions and for simulations across the entire upper hemisphere (top panels) or else restricted to the principal plane only (bottom panels). In general, all panels of Fig. 8 show a good agreement between the BRF values of the reference and reconstructed tree canopies. The BRF deviations are expressed in terms of the RMSD which was calculated with Eq. (5), using simulation results for the observation zenith angle in the range −85° to 85°. The RMSD values vary from 0.001 to 0.0016 in the red and from 0.0020 to 0.0026 in the NIR spectral bands. A comparison with RMSD values generated for the BRF differences of forest canopies generated from one tree model only (results not shown) indicates that discrepancies in the architecture of the model trees were amplified when the forest is composed of one instead of four different tree models.

The results of the radiation transfer simulations indicated that structural differences in individual trees have less of an impact in the NIR than in the red spectral band. Furthermore at spatial scales of 1 ha they were, on average, lying within the absolute calibration accuracy of current moderate resolution space sensors, i.e. 3–5%. The proposed tree reconstruction model is thus well suited to be used in the context of remote sensing product validation over known sites. This opportunity will be discussed further in the following section.

4.2. Comparison of hemispherical photographs

Digital hemispherical photography has long been used to document the architectural properties of plant canopies. A large body of work (e.g., Chen et al., 1991; Fournier et al., 2003; Gower et al., 1999; Bréda, 2003; Jonckheere et al., 2004; Leblanc et al., 2005; Montes et al., 2007) deals with the extraction of structural attributes, like gap fraction and LAI, from hemispherical photographs. The *Rayspread* model was utilised to simulate hemispherical photographs at different locations within the 100 m × 100 m forest stand composed of 4 different tree species. The photographs are segmented, which means that every black and white pixel corresponds to obstruction by material (foliage or wood) or gap in the canopy respectively. Fig. 9 shows two examples of such imagery, acquired at position (30 m, 30 m) and (50 m, 50 m) in the canopy composed of reference tree models (left panels), VIS (middle panels) and FIX reconstructed tree models (right panels). The visually comparison of the various panels in Fig. 9 shows little difference between the photography taken from the stand composed of the reference tree models and the stands composed of the reconstructed tree models. We used the HemiView v2.1 software (www.delta-t.co.uk) to obtain more quantitative information regarding the gap fraction distribution. Fig. 10 shows the azimuthally averaged gap fraction of the hemispherical photographs acquired at position (30, 30; left panels) and (50, 50; right panels). The mean gap fractions values for 5° zenith bins for the reference (solid line), the VIS (white disk) and FIX (grey diamond) reconstructed tree models are indicated. The goodness of fit, already hinted in the hemispherical photographs, is confirmed by the RMSD values which are of the order of 0.01 for position (30, 30) and 0.02 for position (50, 50). The latter is probably due to the presence of a

Table 3
Deviation in percentage of the 250 BRF values distributed over the sky hemisphere and for 54 virtual forest site simulations with the fixed number of shoots (FIX) and visually compared (VIS) reconstructed tree models.

	Deviation of BRF in the red band (%)		Deviation of BRF in the NIR band (%)	
	VIS	FIX	VIS	FIX
Western hemlock	−7.44	−4.75	0.27	−0.64
Aleppo pine	−5.64	−3.88	−1.17	0.09
Douglas fir	0.92	0.85	2.80	1.35
Western red cedar	−3.30	−5.47	−4.36	−3.98

Douglas fir tree, with its lack of wood in both the VIS and FIX case, near the center of the simulated photograph.

5. Discussion and concluding remarks

This study described a modelling approach to reconstruct plausible tree architectures from multiple TLiDAR scans. The main steps of the proposed algorithm consist in 1) segmenting the co-registered 3D point cloud into a predominantly wood and a predominantly foliage components, on the basis of the intensity information of the TLiDAR returns, 2) extracting a skeleton structural frame from the 'wood' point cloud that defines the trunk and first-order branches of the tree model, 3) use the 'foliage' point cloud as an attractor set to grow a finer branching structure from this initial tree skeleton, 4) define a typical foliage (shoot or leaf) structure and add one instance of this object at the terminating end of every branch, and 5) use a light availability model to distribute additional foliage elements within the interior of the tree crown. In this study the reconstruction algorithm was applied only to coniferous trees but nothing prevents its usage with broadleaf tree species.

The main strength of the proposed reconstruction algorithm lies in its capacity to generate plausible tree architectures even when the TLiDAR scans were acquired with low spatial/angular resolutions and/or under non-ideal external conditions, e.g., in the presence of wind and/or occlusions of the interior of the tree crowns. These conditions are particularly aggravating for evergreen coniferous species in that they can never be scanned without their foliage and consequently the fine structural details of needle arrangements inside individual shoots may be below the resolving power of current TLiDAR instruments. The main weakness of the proposed approach lies in the fact that some sort of criteria is required to terminate the foliage addition process. Unfortunately, the co-registered 3D point cloud of the three TLiDAR scans cannot be used for this because it is affected both by viewpoint-related occlusions and wind-induced displacements of branches and foliage in successive TLiDAR acquisitions. In the present study the decision to stop or pursue the generation of tree elements was based on either a visual inspection of the reconstructed tree architecture or by using a priori knowledge of the leaf area of the reference tree. The purpose of this approach was twofold: on the one hand it would provide an indication of the errors that could be expected if a tree was to be reconstructed without a priori information regarding its foliage amount and spatial distribution, and, on the other hand, this would also justify the development of a more refined foliage addition procedure to be applied when the reconstructed tree (constrained to have the correct amount of foliage) still differs from the reference, due the placement of the foliage inside the crown.

It is always possible – although not discussed in detail in this study – to adjust the parameters of the reconstruction model manually, such

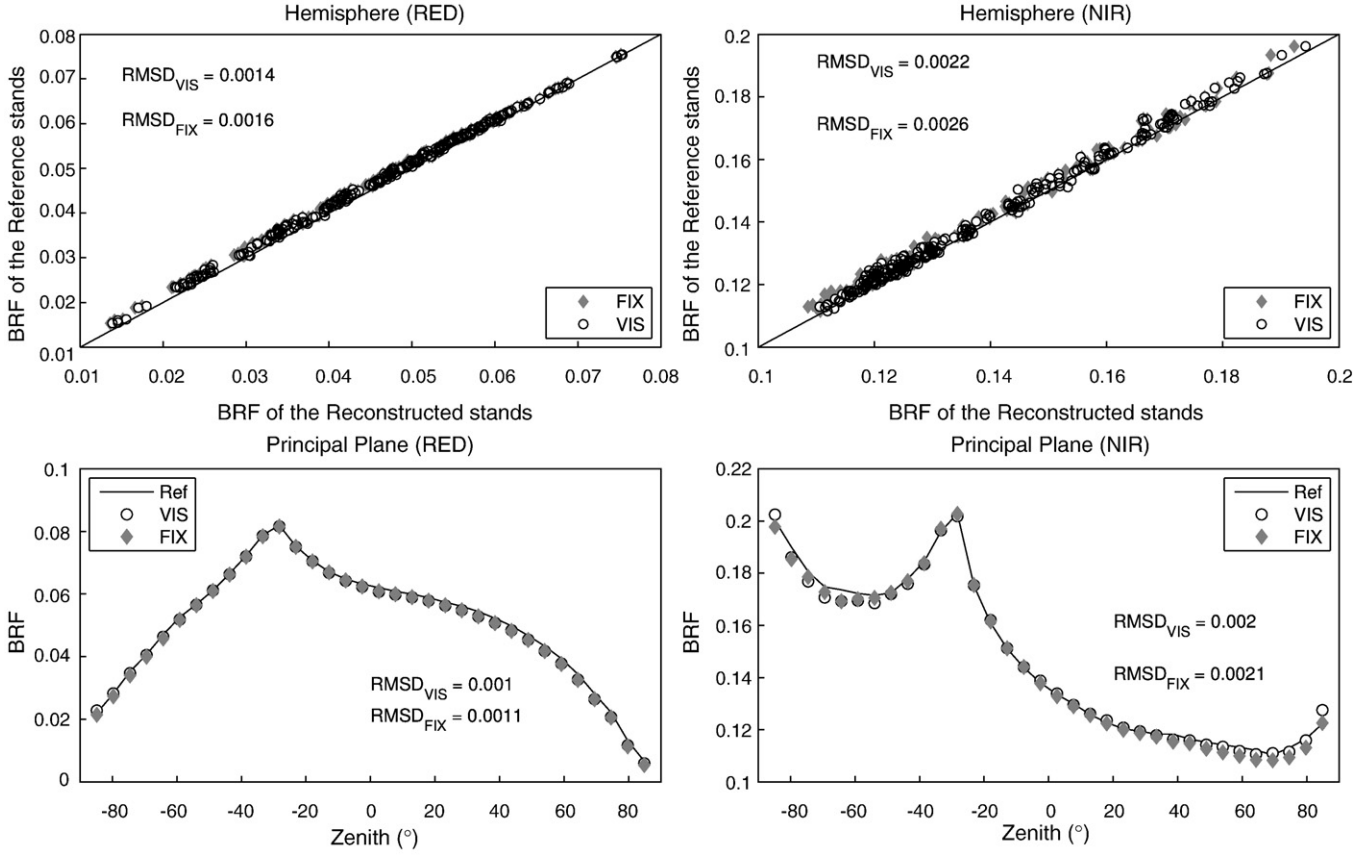

Fig. 8. Bidirectional Reflectance Factor simulated over a virtual forest site composed of the 4 species randomly distributed for the visually compared (VIS) – white disk– and fixed number of shoots (FIX) – grey diamond – reconstructed tree models. Top panels show the BRF simulated for 250 directions uniformly distributed in the upper hemisphere. Bottom panels show the BRF in the principal plane sampled at each 5°. Root mean squared deviations (RMSD) of the distribution are displayed for the visually compared (VIS) and fixed number of shoots (FIX) reconstructed tree models.

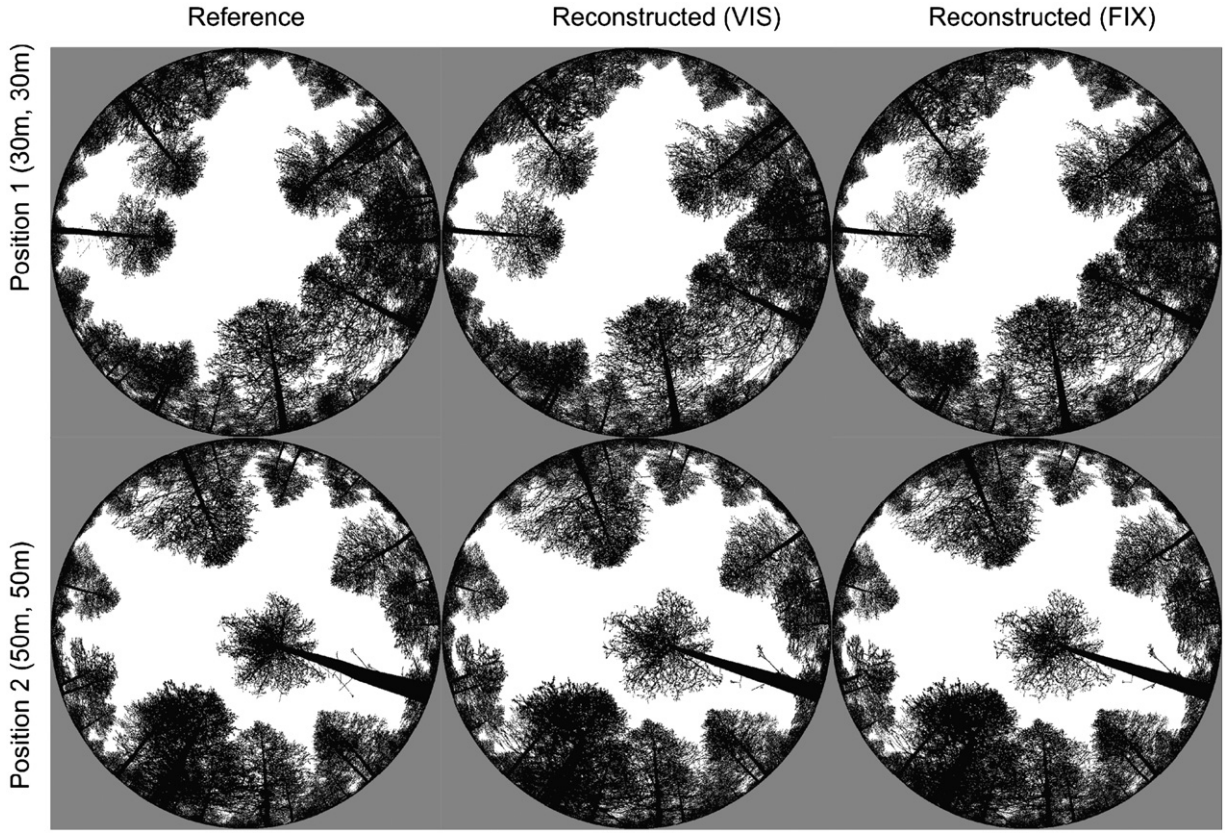

Fig. 9. Threshold hemispherical photographs simulated in a virtual forest stands of 100 m × 100 m built with the reference (left panels) tree models, the visually compared (VIS) (middle panels) and fixed number of shoots (FIX) (right panels) reconstructed tree models.

that they result in a tight fit of the generated tree model and the real tree. For example, the branching structure of the reconstructed tree can be tuned by applying three procedures: (i) removing noise, resolving gaps or connecting disjoint parts in the 3D aligned TLiDAR scans, when possible, using available software or algorithms, to have a 'cleaner' and more detailed initial skeleton, (ii) adequately choosing the attractor set and adjusting the parameters for growing the branching structure and (iii) using the full potential of the L-System formalism with realistic botanical production rules to simulate plant growth according to its species and environment (e.g., tropism, branching pattern, pipe model). Such an approach is, however, labour intensive and prevents also the routine operational use of the proposed tree reconstruction procedure in the systematic interpretation of TLiDAR scans. What is thus needed is an external source of information that could automatically steer the branch construction and foliage addition process, as indicated by the feedback mechanism in Fig. 2. One possible source of such information could be hemispherical photography acquired at the time of the TLiDAR scans. Multiple hemispherical photographs could be used to obtain information on the directional transmission of a target tree, which in turn, could serve 1) to obtain spatially correct distributions of foliage in the crown

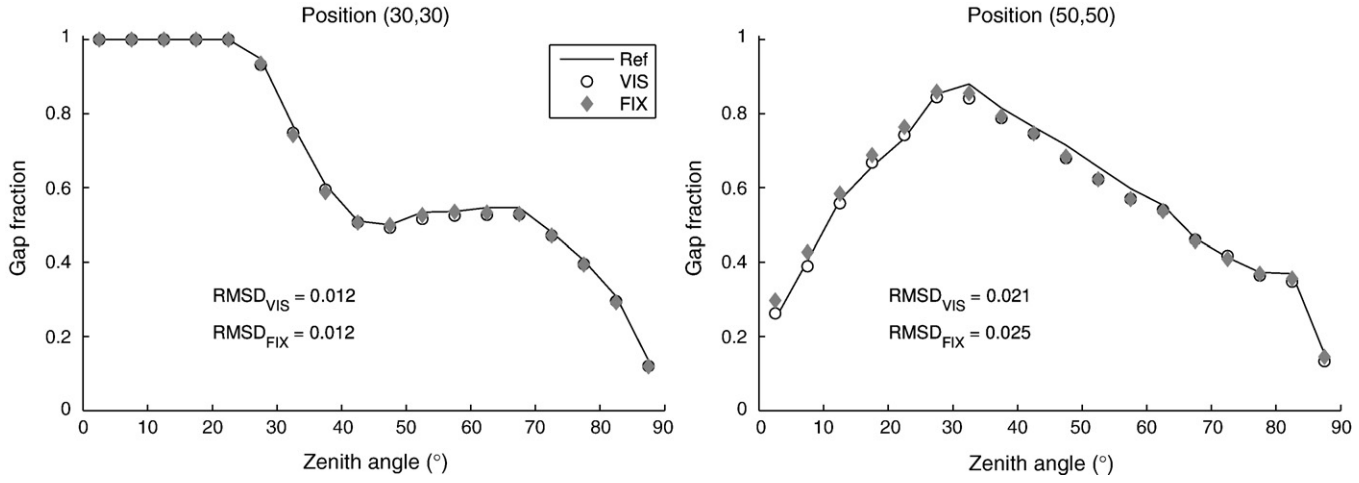

Fig. 10. Gap fraction of hemispherical photographs generated with the HemiView v2.1 software simulated in a 1 ha virtual forest composed of 4 tree species: reference tree models – solid line–, the visually compared (VIS) – white disk– and fixed number of shoots (FIX) – grey diamonds– reconstructed tree models. Root mean squared deviations (RMSD) of the distribution for the visually compared (VIS) and fixed number of shoots (FIX) reconstructed tree models are displayed.

and 2) to terminate the foliage addition process. Future work will have to be directed towards the automation of such a feedback system, perhaps using optimisation algorithms that reduce the differences between key parameters (e.g., directional gap fraction) of the modelled and actual scenarios.

Species-specific conifer shoot models should also be specified in accordance with field measurements, to account for differences amid species as well as site, age and stress related factors. Nevertheless, all four of the tree models reconstructed during this study did exhibit structural properties similar to those of the reference trees used as reference, for instance in terms of the vertical leaf and wood area distribution, as well as the foliage orientation distribution. Far from being exact copies, the reconstructed tree models were capable of delivering accurate stand level reflectance signatures as well as hemispherical photographs acquired at different locations within the canopy. The applicability of our methodology for the reconstruction of 3D architecture of realistic forest canopy remains to be improved. For instance some issues concerning its feasibility remain unresolved. Reconstruction of a single tree or a group of trees in dense forest stands could be problematic if the occlusions by neighbouring trees reduce significant visibility from several view points using the TLiDAR. Therefore we plan to compare RT simulations based on the proposed tree reconstruction method with remote sensing observations over a series of stands with diversified structure to account for the impact of different tree shapes and crown overlap.

The results of our simulations suggest that the tree reconstruction algorithm described above could serve, in conjunction with validated and geometrically explicit 3D radiative transfer models, to support and perhaps even optimise future efforts to validate remotely sensed data and products. Space agencies and scientific networks maintain long term validation or measurement sites, respectively, that could be simulated in great detail with a 3D radiation transfer model, using tree models generated with the proposed methodology. Assuming that information on the leaf, wood, and background spectral properties is also available for these sites, the 3D RT model could be used to predict the surface reflectance or derived products such as FAPAR (Gobron et al., 2006) of that test site, at the time of overpass of a given space borne sensor, given the directional properties of the incident radiation. This would enable 1) a direct comparison with remotely sensed products, 2) a direct comparison with domain-level estimates of radiative quantities (like FAPAR) from up-scaling procedures of in-situ measurements, and 3) the formulation of site-specific sampling strategies optimised for the estimation of domain-level radiative quantities. Considered coniferous forests, with their typical shoot and branch clumping, could continue to serve as test sites, but nothing prevents the same approach from being applied to deciduous forests, where the woody structure can be reconstructed more accurately from winter scans, and where foliage information can be gathered using hemispherical photography throughout the year. The validation of remote sensing products can now be considered using such 3D RT models, driven by an exhaustive set of structural and spectral data acquired in the field, e.g. with TLiDARs. This opportunity should be considered by space agencies, data providers and scientific organisations like the Committee on Earth Observing Satellites (CEOS), as part of their long term validation strategies.

Acknowledgments

We wish to thank Laurent Borgniet of the Institut de recherche pour l'ingénierie de l'agriculture et de l'environnement (CEMAGREF) of Aix-en-Provence (France) for providing equipment and access to the site of Bois des Roussettes where we collected data for the Aleppo pine. Collaboration from Nick Smith (Forest Engineer in British Columbia) and Gordon Frazer (Victoria University) was crucial for access to the site of Malahat and Shawnigan and availability of the three other trees. We would like to thank Richard Egli (Sherbrooke University) for many discussions and insightful advices about the modelling approach. We are also indebted to Guy Côté of MCG3D (Québec, Canada) and, Francis Langelier (coop student at Sherbrooke University) for their help in post-processing data from Malahat and Shawnigan sites. We are grateful to Alan Belward, head of the Global Environment Monitoring unit at the Joint Research Centre of the European Commission, for authorizing the internship of Jean-François Côté at the JRC.

References

Amanatides, J. (1984). Ray tracing with cones. *ACM SIGGRAPH Computer Graphics*, *18*, 129—135.

Barber, C. B., Dobkin, D. P., & Huhdanpaa, H. T. (1996). The Quickhull algorithm for convex hulls. *ACM Transactions on Mathematical Software*, *22*, 469—483.

Besl, P. J., & McKay, N. D. (1992). A method for registration of 3-D shapes. *IEEE Transaction on Pattern Analysis and Machine Intelligence*, *14*, 239—256.

Bréda, N. J. J. (2003). Ground-based measurements of leaf area index: a review of methods, instruments and current controversies. *Journal of Experimental Botany*, *54*, 2403—2417.

Bunnik, N. J. J. (1978). *The multispectral reflectance of shortwave radiation of agricultural crops in relation with their morphological and optical properties.* Mededelingen Landbouwhogeschool The Netherlands: Wageningen 175 pp.

Campbell, G. S., & Norman, J. M. (1990). The description and measurement of plant canopy, structure. In G. Russell, B. Marshall & P. G. Jarvis (Eds.), *Plant canopies: their growth, form, and function* (pp. 1—19). Cambridge: Cambridge University Press.

Chasmer, L., Hopkinson, C., & Treitz, P. (2006). Investigating laser pulse penetration through a conifer canopy by integrating airborne and terrestrial lidar. *Canadian Journal of Remote Sensing*, *32*, 116—125.

Chen, J. M., Black, T. A., & Adams, R. S. (1991). Evaluation of hemispherical photography for determining plant area index and geometry of a forest stand. *Agricultural and Forest Meteorology*, *56*, 129—143.

Cheng, Z. L., Zhang, X. P., & Chen, B. Q. (2007). Simple reconstruction of tree branches from a single range image. *Journal of Computer Science and Technology*, *22*, 846—858.

Cormen, T. H., Leiserson, C. E., & Rivest, R. L. (2001). *Introduction to algorithms.* New York, USA: McGraw-Hill 1216 pp.

Danson, F. M., Hetherington, D., Morsdorf, F., Koetz, B., & Allgöwer, B. (2007). Forest canopy gap fraction from terrestrial laser scanning. *IEEE Geosciences and Remote Sensing Letters*, *4*, 157—160.

Fournier, R. A., Mailly, D., Walter, J. -M. N., & Soudani, K. (2003). Indirect measurement of forest structure from in situ optical sensors. In M. Wulder & S. Franklin (Eds.), *Methods and applications for remote sensing of forests: Concepts and case studies* (pp. 77—114). Norwell, MA: Kluwer Academic Publishers.

Gobron, N., Pinty, B., Aussedat, O., Chen, J., Cohen, W. B., Fensholt, R., et al. (2006). Evaluation of FAPAR products for different canopy radiation transfer regimes: Methodology and results using Joint Research Center products derived from SeaWiFS against ground-based estimations. *Journal of Geophysical Research*, 111. doi:10.1029/2005JD006511.

Godin, C., Costes, E., & Sinoquet, H. (1999). A method for describing plant architecture which integrates topology and geometry. *Annals of Botany*, *84*, 343—357.

Goel, N. S., & Strebel, D. E. (1984). Simple beta distribution representation of leaf orientation in vegetation canopies. *Agronomy Journal*, *76*, 800—803.

Gower, S. T., Kucharik, C. J., & Norman, J. M. (1999). Direct and indirect estimation of leaf area index, fPAR, and net primary production of terrestrial ecosystems. *Remote Sensing Environment*, *70*, 29—51.

Hopkinson, C., Chasmer, L., Young-Pow, C., & Treitz, P. (2004). Assessing forest metrics with a ground-based scanning lidar. *Canadian Journal of Forest Research*, *34*, 573—583.

Hosoi, F., & Omasa, K. (2006). Voxel-based 3-D modeling of individual trees for estimating leaf area density using high-resolution portable scanning lidar. *IEEE Transactions on Geoscience and Remote Sensing*, *44*, 3610—3618.

Hosoi, F., & Omasa, K. (2007). Factors contributing to accuracy in the estimation of the woody canopy leaf area density profile using 3D portable lidar imaging. *Journal of Experimental Botany*, *58*, 3463—3473.

Jonckheere, I., Fleck, S., Nackaerts, K., Muysa, B., Coppin, P., Weiss, M., et al. (2004). Review of methods for in situ leaf area index determination Part I. *Theories, sensors and hemispherical photography. Agricultural and Forest Meteorology*, *121*, 19—35.

Leblanc, S. G., Chen, J. M., Fernandes, R., Deering, D. W., & Conley, A. (2005). Methodology comparison for canopy structure parameters extraction from digital hemispherical photographs in boreal forests. *Agricultural and Forest Meteorology*, *129*, 187—207.

Lovell, J. L., Jupp, D. L. B., Culvenor, D. S., & Coops, N. C. (2003). Using airborne and ground-based ranging lidar to measure canopy structure in Australian forests. *Canadian Journal of Remote Sensing*, *29*, 607—622.

Měch, R., & Prusinkiewicz, P. (1996). Visual models of plants interacting with their environment. Proceedings of SIGGRAPH 96 (New Orleans, Louisiana, August 4–9, 1996). *Computer Graphics Proceedings, Annual Conference Series, ACM SIGGRAPH* (pp. 397—410).

Montes, F., Pita, P., Rubio, A., & Canellas, I. (2007). Leaf area index estimation in mountain even-aged Pinus silvestris L. stands from hemispherical photographs. *Agricultural and Forest Meteorology*, *145*, 215—228.

Omasa, K., Hosoi, F., & Konishi, A. (2007). 3D lidar imaging for detecting and understanding plant responses and canopy structure. *Journal of Experimental Botany*, *58*, 881—898.

Pfeifer, N., Gorte, B., & Winterhalder, D. (2004). Automatic reconstruction of single trees from terrestrial laser scanner data. ISPRS – international archives of photogrammetry. *Remote Sensing and Spatial Information Sciences*, *Vol. XXXV*. (pp. 114—119) Part B5.

Pharr, M., & Humphreys, G. (2004). *Physically based rendering: From theory to implementation.*: Morgan Kaufmann Publishers 1042 pp.

Pinty, B., Gobron, N., Widlowski, J. -L., Gerstl, S. A. W., Verstraete, M. M., Antunes, M., et al. (2001). Radiation transfer model intercomparison (RAMI) exercise. *Journal of Geophysical Research*, *106*, 11937—11956.

Pinty, B., Widlowski, J. -L., Tabermer, M., Gobron, N., Verstraete, M. M., Disney, M., et al. (2004). Radiation Transfer Model Intercomparison (RAMI) exercise: Results from the second phase. *Journal of Geophysical Research*, *109*. doi:10.1029/2003JD004252.

Prusinkiewicz, P., & Lindenmayer, A. (1990). *The algorithmic beauty of plants.* New-York: Springer-Verlag 228 pp.

Runions, A., Lane, B., & Prusinkiewicz, P. (2007). Modeling trees with space colonization algorithm. *Eurographics Workshop on Natural Phenomena 2007* (pp. 63—70).

Shinozaki, K., Yoda, K., Hozumi, K., & Kira, T. (1964). A quantitative analysis of plant form – the pipe theory model. I. basic analyses. *Japanese Journal of Ecology*, *14*, 97—105.

Simonse, M., Aschoff, T., Spiecker, H., & Thies, M. (2003). Automatic determination of forest inventory parameters using terrestrial laserscanning. *Proceedings of the ScandLaser Scientific Workshop on Airborne Laser Scanning of Forests. Umeå* (pp. 251—257).

Smolander, S., & Stenberg, P. (2003). A method to account for shoot scale clumping in coniferous canopy reflectance models. *Remote Sensing Environment*, *88*, 363—373.

Taylor-Hell, J. (2005). Biomechanics in Botanical Trees. M.Sc. thesis, University of Calgary, Canada.

Verroust, A., & Lazarus, F. (2000). Extracting skeletal curves from 3D scattered data. *The Visual Computer*, *16*, 15—25.

Xu, H., Gossett, N., & Chen, B. (2007). Knowledge and heuristic-based modeling of laser-scanned trees. *ACM Transactions on Graphics*, *26*. doi:10.1145/1289603.1289610.

Widlowski, J. -L., Lavergne, T., Pinty, B., Verstraete, M., & Gobron, N. (2006). Rayspread: A virtual laboratory for rapid BRF simulations over 3-D plant canopies. In F. Graziani (Ed.), *Computational Methods in Transport* (pp. 211—231). Berlin: Springer.

Widlowski, J. -L., Robustelli, M., Disney, M., Gastellu-Etchegorry, J. -P., Lavergne, T., Lewis, P., et al. (2008). The RAMI On-line Model Checker (ROMC): A web-based benchmarking facility for canopy reflectance models. *Remote Sensing of Environment*, *112*, 1144—1150.

Widlowski, J. -L., Taberner, M., Pinty, B., Bruniquel-Pinel, V., Disney, M., Fernandes, R., et al. (2007). The third RAdiation transfer Model Intercomparison (RAMI) exercise: Documenting progress in canopy reflectance modelling. *Journal of Geophysical Research*, 112. doi:10.1029/2006JD007821.